

MICROCOPY RESOLUTION TEST CHART  
NATIONAL BUREAU OF STANDARDS-1963-A



THE ROLE OF EIGENSOLUTIONS IN  
NONLINEAR INVERSE CAVITY-FLOW  
THEORY

B. R. Parkin

AD-A151 473

Technical Memorandum  
File No. TM 85-16  
25 January 1985  
Contract N00024-79-C-6043

Copy No. 2

The Pennsylvania State University  
Intercollege Research Programs and Facilities  
APPLIED RESEARCH LABORATORY  
Post Office Box 30  
State College, Pa. 16804

DTIC FILE COPY

NAVY DEPARTMENT  
NAVAL SEA SYSTEMS COMMAND

DTIC  
ELECTE  
MAR 20 1985  
S  
A A

85 03 07 174

THE ROLE OF EIGENSOLUTIONS IN  
NONLINEAR INVERSE CAVITY-FLOW  
THEORY

B. R. Parkin

Technical Memorandum  
File No. TM 85-16  
25 January 1985  
Contract N00024-79-C-6043

Copy No. 2

Approved for public release  
Distribution unlimited

The Pennsylvania State University  
Intercollege Research Programs and Facilities  
APPLIED RESEARCH LABORATORY  
Post Office Box 30  
State College, PA 16804

NAVY DEPARTMENT

NAVAL SEA SYSTEMS COMMAND

S MAR 20 1985

A

UNCLASSIFIED

SECURITY CLASSIFICATION OF THIS PAGE (When Data Entered)

REPORT DOCUMENTATION PAGE		READ INSTRUCTIONS BEFORE COMPLETING FORM
1. REPORT NUMBER TM 85-16	2. GOVT ACCESSION NO.	3. RECIPIENT'S CATALOG NUMBER
4. TITLE (and Subtitle) THE ROLE OF EIGENSOLUTIONS IN NONLINEAR INVERSE CAVITY-FLOW THEORY		5. TYPE OF REPORT & PERIOD COVERED Technical Memorandum
		6. PERFORMING ORG. REPORT NUMBER
7. AUTHOR(s) B. R. Parkin		8. CONTRACT OR GRANT NUMBER(s) N00024-79-C-6043
9. PERFORMING ORGANIZATION NAME AND ADDRESS Applied Research Laboratory, P.O. Box 30 The Pennsylvania State University State College, PA 16804		10. PROGRAM ELEMENT, PROJECT, TASK AREA & WORK UNIT NUMBERS
11. CONTROLLING OFFICE NAME AND ADDRESS Naval Sea Systems Command, Code NSEA 63R31 Department of the Navy Washington, DC 20362		12. REPORT DATE 25 January 1985
		13. NUMBER OF PAGES 52
14. MONITORING AGENCY NAME & ADDRESS (if different from Controlling Office) David W. Taylor Naval Ship R&D Center Code 1542 Department of the Navy Bethesda, MD 20084		15. SECURITY CLASS. (of this report) UNCLASSIFIED
		15a. DECLASSIFICATION, DOWNGRADING SCHEDULE
16. DISTRIBUTION STATEMENT (of this Report) Approved for public release. Distribution unlimited. Per NAVSEA - 25 February 1985.		
17. DISTRIBUTION STATEMENT (of the abstract entered in Block 20, if different from Report)		
18. SUPPLEMENTARY NOTES		
19. KEY WORDS (Continue on reverse side if necessary and identify by block number) cavity flows inverse hydrofoil design mathematical properties,		
20. ABSTRACT (Continue on reverse side if necessary and identify by block number) The method of Levi Civita is applied to an isolated fully cavitating body at zero cavitation number and adapted to the solution of the inverse problem in which one prescribes the pressure distribution on the wetted surface and then calculates the shape. The novel feature of this work is the finding that the exact theory admits the existence of a "point drag" function or eigensolution. While this fact is of no particular		

UNCLASSIFIED

SECURITY CLASSIFICATION OF THIS PAGE(When Data Entered)

importance in the classical direct problem, we already know from the linearized theory that the eigensolution plays an important role.

In the present discussion, the basic properties of the exact "point-drag" solution are explored under the simplest of conditions. In this way, complications which arise from non-zero cavitation numbers, free surface effects, or cascade interactions are avoided. The effects of this simple eigensolution on hydrodynamic forces and cavity shape are discussed.

*References*  
*20*

ADMISSION FOR  
CLASSIFIED  
TAB  
SECURITY  
CLASSIFIED

AT

UNCLASSIFIED

SECURITY CLASSIFICATION OF THIS PAGE(When Data Entered)

From: B. R. Parkin

Subject: The Role of Eigensolutions in Nonlinear Inverse  
Cavity-Flow Theory

Abstract: The method of Levi Civita is applied to an isolated fully cavitating body at zero cavitation number and adapted to the solution of the inverse problem in which one prescribes the pressure distribution on the wetted surface and then calculates the shape. The novel feature of this work is the finding that the exact theory admits the existence of a "point drag" function or eigensolution. While this fact is of no particular importance in the classical direct problem, we already know from the linearized theory that the eigensolution plays an important role.

In the present discussion, the basic properties of the exact "point-drag" solution are explored under the simplest of conditions. In this way, complications which arise from non-zero cavitation numbers, free surface effects, or cascade interactions are avoided. The effects of this simple eigensolution on hydrodynamic forces and cavity shape are discussed.

Acknowledgments: This work has been supported by the Naval Sea Systems Command, Dr. Thomas E. Peirce [Code NSEA 63R31], and by the David W. Taylor Naval Ship Research & Development Center [DTNSRDC] under the General Hydrodynamics Research Program. The author is particularly pleased to acknowledge the helpful discussions of this work by Dr. Y. T. Shen of DTNSRDC.

Principal Nomenclature

$A_1$	cavity detachment point near or at profile nose
$A_2$	cavity detachment point at profile trailing edge
$a = (\sqrt{\phi_1} - \sqrt{\phi_2})/2$	see related nomenclature below
$b = (\sqrt{\phi_2} + \sqrt{\phi_2})/2$	see related nomenclature below
$C$	location of eigensolution singularity on unit circle
$C_D$	drag coefficient
$C_L$	lift coefficient
$C_p(\beta)$	pressure coefficient on wetted surface
$c$	profile chord length, $c = 1$
$ds$	element of arc length in $z$ -plane
$E$	strength of eigensolution
$F = \phi + i\psi$	complex potential and complex $F$ -plane
$\phi$	velocity potential
$\psi$	stream function
$C$	stagnation point location
$O'$	point at infinity in $z$ -plane
$U$	free-stream velocity
$W$	intermediate mapping complex plane
$w = u - iv = \frac{dF}{dz}$	complex velocity
$Z$	intermediate mapping complex plane
$z = x + iy$	complex variable in the physical $(x,y)$ plane

$\alpha$	angle of attack
$\delta$	angular location of stagnation point measured from negative real axis
$\zeta$	dummy variable
$\eta$	normal effect from profile chord
$\xi$	complex semi-circle plane, $\xi = e^{i\beta}$
$\sigma$	distance along profile chord
$\tau$	cavity thickness at trailing edge
$\gamma$	stagnation point angular location on unit circle in $\zeta$ plane ( $\cos \gamma = a/b$ )
$\gamma_c$	angular location of eigensolution singularity on unit circle
$\phi_1$	value of $\phi$ at $A_1$
$\phi_2$	value of $\phi$ at $A_2$
$\omega(\zeta) = \theta + i \ln q/U = \theta + i\tau$	complex logarithmic hodograph
$\theta$	flow inclination
$q$	flow speed

Subscripts

0	pertains to flat plate solution $\omega_0$
1	pertains to regular part of solution $\omega_1$
c	pertains to eigensolution $\omega_c$

## Introduction

The present paper bears upon the two-dimensional inverse or design problem for fully-cavitating hydrofoils in which one specifies the pressure distribution on the profile wetted surface and then calculates that wetted surface shape which will satisfy this prescription. This design problem is certainly not new to airfoil designers and as far as cavity flows are concerned, both linear and nonlinear design methods have been worked out. In the realm of nonlinear approaches to the problem, the very general method of Yim and Higgins [1]\* is worthy of note because it applies to single foils as well as to cascades of profiles for all cavitation numbers in the cavity-flow regime. Another approach has been discussed superficially by Khrabov [2]. Both of these contain far more generality than is required for this study at zero cavitation number. For the direct or off-design problem of exact cavity-flow theory, a good example of the present level of development is represented by the work of Furuya [3] and it is clear that now one can do both the design and off design problems for fully-cavitating hydrofoils. Thus, one can attempt to tailor the profile to an entire set of performance goals and failing that he can at least design for the best compromise among a set of conflicting requirements.

According to many authors [4-7], the inverse problem is not thought to present much of a challenge at zero cavitation number. In this case, the classical method of Levi Civita [7] can be applied to an isolated

---

\*Numbers in square brackets indicate citations in the references listed below.

body. This view is certainly proper as long as one is content, after prescribing the pressure in the circle plane, to accept whatever correlation between points in the circle and physical planes may result. Of course, such a rudimentary approach does not lead to a useful design procedure.

The motivation for the present investigation is that none of the literature on the nonlinearized inverse problem we have surveyed so far [1-8] has made use of the fact the exact theory admits the existence of a "point drag" or complementary function. While this fact is of no particular importance in the direct problem, we have already seen in the case of the linearized inverse problem [9-11] that the complementary function can play an important role. For the exact theory there has been a question if a nonlinear eigensolution exists [1]. Therefore, in this study, we explore the question regarding the existence of a "point drag" or eigensolution in the nonlinear theory under the simplest set of circumstances and this leads us naturally to the restrictions that the free streamline flow pertains to an isolated profile and that the flow be at zero cavitation number. These simplifications will free us from the complications arising from non-zero cavitation numbers and other boundaries in the flow domain such as a free surface or neighboring cascade blades.

In this paper we use the term eigensolution in the sense of thin airfoil theory as suggested by the work of Van Dyke\* because we already know that the inverse problem in the theory of fully cavitating hydrofoils

---

\*Perturbation Methods in Fluid Mechanics, The Parabolic Press, Stanford, CA, pp. 48-54 (1975).

is not necessarily unique. Our aim is to find a sufficiently weak singularity which can be added to the classical Levi Civita solution and can then be used to satisfy certain additional physical conditions relating to the location of the free streamline springing from the hydrofoil nose and thereby provide a unique inverse cavity-flow solution. After we have constructed the simple eigensolution, we will examine some of its properties. The use of this solution in the design process will be presented elsewhere.

#### Flow Geometry and Conformal Mappings

As noted above, this study uses Levi Civita's method [7] for the analysis of the exact inverse problem for a fully cavitating hydrofoil section. The flow geometry and the principal quantities associated with the flow are illustrated in Fig. 1. The origin of coordinates in the  $z = x + iy$  plane is taken at the stagnation point on the wetted surface of the hydrofoil. This point is denoted by  $O$  in Fig. 1. The chordline of the profile is inclined at the angle  $\alpha$  with respect to the  $x$  axis and the free-stream velocity  $U$  is taken as being parallel to this axis as illustrated. The flow separation point at or near the profile nose is the point  $A_1$  as illustrated for a sharp-nosed foil. The "upper" cavity surface is shown as the dashed curve extending from  $A_1$  to the point  $O'$  at downstream infinity. In the case of a round-nose profile  $A_1$  can lie on the upper wetted surface behind the leading edge. This case is not illustrated in Fig. 1. The point  $A_2$  denotes the location of the trailing edge of the wetted surface. The lower surface of the cavity leaves the wetted surface at  $A_2$  and extends as shown by the dashed line to the point  $O'$  at downstream infinity.

Let the coordinates of a typical point on the wetted surface be denoted by  $\bar{x}$  and  $\bar{y}$  and those on the upper cavity by  $x_c$  and  $y_c$  as shown in Fig. 1. While the orientation of the profile in the  $z$  plane is convenient for the purposes of analysis, the  $x$ - $y$  system is not always a convenient reference frame for foil and cavity contours. For this purpose we use a coordinate system with the abscissa along the chordline as shown by the distance  $\sigma$  measured from the profile nose. The ordinates of the wetted surface are then given in terms of  $\sigma$  as  $\eta(\sigma)$  and the upper cavity ordinates are given by  $\eta_c(\sigma)$ . At the trailing edge of the profile, the cavity thickness is  $\eta_c = T$ . These quantities are also shown in Fig. 1. In the  $\sigma, \eta$  system the stagnation point  $O$  is located at  $(\sigma_0, \eta_0)$  as illustrated. The transformation between the  $(x, y)$  and  $(\sigma, \eta)$  systems is

$$\sigma + i\eta = \sigma_0 + i\eta_0 + ze^{i\alpha} \quad , \quad (1)$$

where  $z$  is the complex variable,  $z = x + iy$ , and  $\alpha$  is the angle-of-attack as measured by the inclination of the chordline with respect to the  $x$  axis and free-stream velocity  $U$ .

The conformal mappings start with the complex potential in the  $z$ -plane,

$$F = \phi + i\psi \quad , \quad (2)$$

where  $\phi$  is the velocity potential and  $\psi$  is the stream function. As is customary, we adjust these quantities to make  $\phi = 0$  at the stagnation point,  $O$ . The stream function is taken to be zero all along the stagnation streamline. Therefore, the boundaries of the flow can be represented by a cut all along the real axis in the  $F$ -plane as shown in Fig. 2. Note that the wetted surface extends from the stagnation point

at 0 to the trailing edge at  $A_2$  and the lower cavity surface from  $A_2$  to  $0'$  must lie along the lower surface of the cut. This is so because downstream from the stagnation point, the velocity potential increases in the flow direction and the stream function decreases outward from the foil or cavity surface. On the arc  $OA_1$ , the flow direction is reversed with a consequent reversal in the gradients of  $\phi$  and  $\psi$  so that the point  $A_1$  is on the upper edge of the cut.

One can use the mapping,

$$W = \sqrt{F} \quad (3)$$

in order to map the  $F$ -plane outside the cut into the upper half of the  $W$ -plane. Corresponding points are shown by the locations of  $0'$ ,  $A_1$  and  $A_2$  and  $0'$  in Fig. 3. As before, the cavity surfaces are shown as dashed lines and the wetted surface is shown by the solid line. Let the values of  $\phi$  at  $A_1$  and  $A_2$  in the  $F$ -plane be  $\phi_1$  and  $\phi_2$  respectively. Then these points are at  $W = \sqrt{\phi_1}$  and  $W = -\sqrt{\phi_2}$  and the midpoint of the distance between  $A_1$  and  $A_2$  is located at

$$W = a = \frac{\sqrt{\phi_1} - \sqrt{\phi_2}}{2} . \quad (4)$$

The distance between this midpoint and  $A_1$  is

$$b = \frac{\sqrt{\phi_1} + \sqrt{\phi_2}}{2} . \quad (5)$$

These distances are also shown in Fig. 3.

$$dz = \frac{dF}{U} e^{i\omega c} = \frac{d(\sqrt{F^2})}{U} e^{iE/\sqrt{F}} .$$

If we put  $t = E/\sqrt{F}$ , we find for a profile of unit chord that

$$dz = -\frac{2E^2}{U} \frac{1}{t^3} e^{it} dt = -\frac{C_D}{\pi} \frac{1}{t^3} e^{it} dt$$

which has the indefinite integral,

$$z = \frac{E^2}{U} \left\{ \frac{e^{it}}{t^2} + i \frac{e^{it}}{t} + \int \frac{e^{it}}{t} dt \right\} . \quad (36)$$

Completion of this integration can be carried out in four parts starting from either side of the stagnation point where  $z = 0$  and  $t \rightarrow \infty$ .

For example, on the arc  $OA_1$  we recall that  $\beta > \gamma$ . Put  $t = t_1$ ,  $\gamma = \pi - \delta$  and  $\beta_1 = \pi - \xi_1$  then

$$t_1 = \frac{E}{b(\cos \xi_1 - \cos \delta)} .$$

Because  $0 < \xi_1 < \delta$ , we have

$$\frac{E}{b(1 - \cos \delta)} < t_1 < \infty .$$

After separating Eq. (36) into real and imaginary parts, we find for this part of the wetted surface, the coordinates

$$\tau_c = 0$$

and

$$\theta_c(\beta) = \frac{E}{b[\cos \gamma - \cos \beta]} = \frac{-E}{2b \sin \frac{\gamma + \beta}{2} \sin \frac{\gamma - \beta}{2}} \quad (35)$$

Since  $\tau_c = 0$  on the wetted surface, we expect  $\omega_c$  to make no contribution to the lift although the singularity at the stagnation point should lead to a drag force. Making use of Eqs. (21), (22) and (34a), we find that

$$C_{L_c} = 0$$

and

$$C_{D_c} = 2\pi \frac{E^2}{Uc}$$

From Eq. (35) we see that the flow direction is not defined at the stagnation point,  $\beta = \gamma$ . However, if  $\beta < \gamma$

$$\theta_c = -\frac{E}{b[\cos \beta - \cos \gamma]} < 0$$

along the arc  $OA_2$ . If  $\beta > \gamma$

$$\theta_c = \frac{E}{b[\cos \gamma - \cos \beta]} > 0$$

Along the arc  $OA_1$ . Therefore  $\theta_c$  changes sign at  $\beta = \gamma$ .

The shape of the wetted and cavity surfaces follows from the relationships of Eq. (14) which can be expressed as

$$\omega_c = \theta_c + i\tau_c = \frac{E}{\sqrt{F}} \quad (33)$$

where  $E$  is a real constant, we have a function which satisfies the necessary requirements. The two conditions  $\omega_c(\infty) = 0$  and  $q_c = U$  on both the cavity and the profile wetted surface can be satisfied by any member of the family of functions having the form  $F^{-m}$ ,  $0 < m < 1$ . But the condition  $\theta_c = 0$  along the entire stagnation streamline can be satisfied only when  $m = 1/2$ . This choice for the complementary function seems to offer the advantage that it will cause less alteration of the upstream flow field inclination than other possibilities. Moreover, it appears to be the most convenient choice for further analysis. Consequently, we shall adopt this functional form for the eigensolution in this work.

Equation (10) can be used to obtain the corresponding representation for  $\omega_c$  in the  $\zeta$ -plane as

$$\omega_c = \frac{E}{b[\cos \gamma - \frac{1}{2}(\zeta + \frac{1}{\zeta})]} = \frac{-2E\zeta}{b(\zeta - e^{i\gamma})(\zeta - e^{-i\gamma})} \quad (34a)$$

In the  $\zeta$ -plane  $\omega_c(0) = 0$  and when  $\zeta$  is real  $\omega_c$  is real. Moreover,  $\omega_c(\zeta)$  is an analytic function which is regular inside the unit circle and which has simple poles at  $\zeta = e^{\pm i\gamma}$ . Note from Eq. (34a) that on the "nose cavity"  $\theta_c \rightarrow 0+$  as  $\zeta \rightarrow -0$  and on the "tail cavity"  $\theta_c \rightarrow 0-$  as  $\zeta \rightarrow +0$ , as illustrated in Fig. 1 also. From Eq. (14),  $w_c = Ue^{-i\omega_c}$  and we see that the structure of  $\omega_c$  leads to an essential singularity in  $w_c$  at the stagnation point 0. The complex velocity  $w_c$  is bounded at this point however, and a smooth foil contour will pass through  $z = 0$ . At points on the unit circle,  $\zeta = e^{i\beta}$ , we have

These results will be used in order to start the functional iteration after the formulation of the theory has been completed. As a final note, we observe that the cavity thickness at the trailing edge of a flat plate according to linearized theory [13] is

$$\eta_c(1) = 1.681\alpha ,$$

which can be compared to the corresponding expression from Eq. (31b). Within the range of attack angles considered here the trailing edge cavity thickness at zero cavitation number is about the same when estimated by linearized or nonlinear theory. For larger values of attack angle we would expect estimates from linearized theory to exceed nonlinear cavity thicknesses.

The flat-plate function  $\omega_0(\zeta)$  is traditionally considered to possess all of the singular behavior of the function  $\omega(\zeta)$ . The shape of the smooth body is then represented by an analytic function  $\omega_1(\zeta)$  which is regular inside and on the unit circle. It must also satisfy the same symmetry requirements as are imposed upon  $\omega_0$  and we must also insist that  $\omega_1(0) = 0$ . Then one traditionally puts  $\omega(\zeta) = \omega_0 + \omega_1$ . As mentioned previously, we will add to this customary sum a new function,  $\omega_c(\zeta)$ , which is the analog of the point-drag function of linearized theory. We will now explore the properties of this eigensolution.

#### The Eigensolution

The complementary function  $\omega_c = \theta_c + i\tau_c$ , is to be determined from the requirements that  $\tau_c = 0$  on the cavity and the foil,  $\theta_c = 0$  along the stagnation streamline and that  $\omega_c$  vanishes at infinity. A function of the form which satisfies these conditions can be found most easily by considering the flow in the F-plane, Fig. 2. If we take

Equation (28) gives the value of  $\frac{b^2}{U}$  to be used in Eqs. (29) and (30).

It is useful to find the ordinate of the upper surface of the cavity above the trailing edge of the wetted surface. This can be done by calculating the quantity

$$f(\zeta_c, \alpha) = \frac{(1 - \zeta_c)^2}{\zeta_c} \left[ \frac{(1 - \zeta_c)^2}{2\zeta_c} \cos \alpha - 2 \right]$$

for several values of  $\zeta_c$  and prescribed values of  $\alpha$ . Then when  $\sigma_c = 1$ , one can plot contours of  $\alpha = \text{constant}$  in an  $f - \zeta_c$  plane and note for each value of  $\alpha$  the value of  $\zeta_c$  corresponding to  $f = 2(4 + \pi \sin \alpha)$ . These values of  $\zeta_c$  can then be used in Eq. (30) in order to compute the value of  $\eta_c(1)$  for each value of  $\alpha$ . It was found when these points were plotted in an  $\eta_c(1) - \alpha$  plane that a linear relationship fits the data for  $0 < \alpha < 10^\circ$ . When  $\alpha$  is measured in degrees this line has the equation

$$\eta_c(1) = .2939\alpha^\circ \quad . \quad (31a)$$

The corresponding relationship for  $\alpha$  measured in radians is

$$\eta_c(1) = 1.684\alpha \quad . \quad (31b)$$

The computed results are tabulated below.

Table 1. Cavity Thickness at the Trailing Edge of a Flat Plate

<u><math>\alpha^\circ</math></u>	<u><math>\zeta_c(1)</math></u>	<u><math>\eta_c(1)</math></u>
0.0	-----	.0000
0.5	.1712	.0147
1.0	.1707	.0297
2.0	.1698	.0585
3.0	.1689	.0879
4.0	.1680	.1174
5.0	.1669	.1463
7.0	.1650	.2049
10.1	.1620	.2939

Additional properties of the flat-plate solution which are important for the present considerations relate to the shape of the upper surface of the cavity. In Fig. (5)  $\zeta$  will be on the negative real axis for points on this part of the cavity. Therefore, let us put  $\zeta = -\zeta_c$  where  $\zeta_c$  is a real positive number. Then we can use  $d(\sigma + i\eta) = e^{i\alpha} dz$ , and write Eq. (17) in the form

$$d(\sigma + i\eta) = \frac{b^2}{U} \exp i[\alpha + \theta_0(\zeta_c)] d\left\{\left[\frac{1}{2}\left(\zeta_c + \frac{1}{\zeta_c}\right) - \cos \alpha\right]^2\right\} .$$

But now

$$\exp i[\alpha + \theta_0] = e^{-i\alpha}(e^{i\alpha} - \zeta_c)/(e^{-i\alpha} - \zeta_c)$$

and so we have

$$d(\sigma + i\eta) = \frac{1}{2} \frac{b^2}{U} [\zeta_c e^{-i\alpha} - 2 + (2i \sin \alpha)/\zeta_c + 2/\zeta_c^2 - e^{i\alpha}/\zeta_c^3] d\zeta_c .$$

The integration in this case starts at  $A_1$  where  $\zeta_c = 1$  and  $\sigma = \eta = 0$  and proceeds to some value of  $\sigma_c, \eta_c$  corresponding to  $1 < \zeta < 0$ . This leads to the parametric representation of  $\eta_c(\sigma_c)$  in terms of  $\zeta_c$  which is given by

$$\sigma_c = \frac{1}{2} \frac{b^2}{U} \frac{(1 - \zeta_c)^2}{\zeta_c} \left[ \frac{(1 + \zeta_c)^2}{2\zeta_c} \cos \alpha - 2 \right] \quad (29)$$

and

$$\eta_c = \frac{1}{2} \frac{b^2}{U} \sin \alpha \left[ \frac{1 - \zeta_c^4}{2\zeta_c^2} + 2 \ln \zeta_c \right] \quad (30)$$

$$dz = -\frac{b^2}{U} \frac{(\cos \xi - \cos \alpha)}{|\cos \xi - \cos \alpha|} e^{i\theta} [(\cos \xi - \cos \alpha)^2 + (\sin \xi + \sin \alpha)^2 \sin \xi] d\xi$$

$$= -e^{i\theta} \operatorname{sgn}(\cos \xi - \cos \alpha) 2 \frac{b^2}{U} [\sin \xi + \sin \alpha \sin^2 \xi - \cos \alpha \cos \xi \sin \xi] d\xi .$$

We can dispose of the product  $-e^{i\theta} \operatorname{sgn}(\cos \xi - \cos \alpha)$  by observing that on the wetted surface when  $0 < \xi < \alpha$  the flow direction is  $\theta = \pi - \alpha$  and when  $\alpha < \xi < \pi$ ,  $\theta = -\alpha$ . Therefore in the first of these cases,  $e^{i\theta} = -e^{-i\alpha}$  and in the second  $e^{i\theta} = +e^{-i\alpha}$ . Hence in either of them the product  $-e^{i\theta} \operatorname{sgn}(\cos \xi - \cos \alpha) = e^{-i\alpha}$ . Next we can introduce  $d(\sigma + i\eta) = e^{i\alpha} dz$  from Eq. (1) with the result that

$$d(\sigma + i\eta) = 2 \frac{b^2}{U} [\sin \xi + \sin \alpha \sin^2 \xi - \cos \alpha \cos \xi \sin \xi] d\xi .$$

This last result implies that  $\eta = 0$  as is proper for a flat plate and  $d\sigma$  is simply the arc length  $ds$  along the wetted surface measured from the profile nose where  $\sigma = 0$ . We can integrate this last equation from  $\sigma = 0$  ( $\xi = 0$ ) to some value,  $0 < \sigma < 1$  ( $0 < \xi < \pi$ ), and get

$$s = 2 \frac{b^2}{U} \left[ (1 - \cos \xi) \left( 1 - \frac{\cos \alpha}{2} [1 + \cos \xi] \right) + (\xi - \sin^2 \xi) \frac{\sin \alpha}{2} \right] . \quad (27)$$

However, the profile is to have unit chord so that when  $\xi = \pi$ ,  $\sigma = s = 1$  and

$$\frac{b^2}{U} = \frac{1}{4 + \pi \sin \alpha} . \quad (28)$$

When Eq. (28) is used in Eqs. (24) and (25), one obtains the well known Rayleigh formulae [12].

$$C_{D_0} = 2\pi \frac{b^2}{Uc} \sin^2 \alpha \quad (25)$$

and we see that  $L/D = \cot \alpha$  as is proper for the flat plate. We can also use the relationship  $C_p = 1 - e^{2\tau}$  to find the pressure distribution on the plate. The result is

$$C_{p_0} = - \frac{4 \sin \beta \sin \gamma}{(\cos \beta - \cos \gamma)^2 + (\sin \beta + \sin \gamma)^2} \quad (26)$$

From this result, we see that when  $\beta = \gamma$ ,  $C_{p_0} = 1$  and when  $\beta = 0$  or  $\pi$ ,  $C_{p_0} = 0$  as required.

Continuing the study of the flat-plate solution, we can rewrite Eq. (23) for points on the wetted surface as

$$\omega_0 = \pi - \alpha + \gamma + i \ln \left[ \frac{e^{i\gamma} - e^{i\beta}}{e^{-i\gamma} - e^{i\beta}} \right] ,$$

in which case

$$e^{\tau_0} = \left| \frac{e^{i\gamma} - e^{i\beta}}{e^{-i\gamma} - e^{i\beta}} \right| = \sqrt{1 - C_{p_0}} \quad .$$

After some manipulation we find that

$$\sqrt{1 - C_{p_0}} = \frac{2 |\cos \beta - \cos \gamma|}{(\cos \gamma - \cos \beta)^2 + (\sin \gamma + \sin \beta)^2} \quad .$$

Next we can put  $\beta = \pi - \xi$  and  $\gamma = \pi - \alpha$  in this expression and in Eq. (17) when it is written for points on the wetted surface. That is,

the real part of the analytic function  $i \ln(\zeta - e^{i\gamma})$ . However this function by itself does not have the proper symmetry needed for admissible forms of  $\omega$ . But if we subtract from it a similar function which has a like jump at the image of 0 with respect to the real axis in the  $\zeta$ -plane, we preserve the necessary behavior at 0 and also satisfy the preceding symmetry requirements. Aside from arbitrary additive constants, this function has the form

$$i \ln \frac{\zeta - e^{i\gamma}}{\zeta - e^{-i\gamma}} .$$

Finally, we require that  $\omega(0) = 0$ . Because of this condition the resulting function which provides the flat plate solution is [4]

$$\omega_0(\zeta) = \theta_0 + i\tau_0 = -\alpha + i \ln \frac{\zeta - e^{i\gamma}}{1 - \zeta e^{i\gamma}} , \quad (23)$$

with  $\gamma = \pi - \alpha$  in the case of an isolated flat-plate profile. For this case, one can show that this function has the flow direction,  $\theta_0 = -\alpha$  or  $\theta_0 = \pi - \alpha$  on  $\zeta = e^{i\beta}$ . Therefore, the wetted surface in the  $z$ -plane is a straight line through 0 with its trailing edge inclined at the angle  $-\alpha$  with respect to the positive real axis. Moreover, since  $\tau_0$  vanishes on the real axis in the  $\zeta$ -plane, the free streamlines have  $C_p = 0$  as required.

The contribution of  $\omega_0$  to  $C_L$  and  $C_D$  follows from Eqs. (21) and (22). From Eqs. (21), (22) and (23) we get

$$C_{L0} = 2\pi \frac{b^2}{Uc} \sin \alpha \cos \alpha \quad (24)$$

$$\tau(-\beta) = -\tau(\beta)$$

and

$$\theta(-\beta) = \theta(\beta) .$$

Hence  $\tau$  is an odd function of  $\beta$ , or  $\text{Im } \zeta$ , and  $\theta$  is an even function of  $\beta$ , or  $\text{Im } \zeta$ .

Using the result,

$$e^\tau = \sqrt{1 - C_p} \quad (20)$$

as noted above, and the fact that  $\omega(\zeta)$  is now defined inside the unit circle one finds [7] from the calculus of residues that

$$C_L = \frac{\pi}{2} \frac{b^2}{Uc} [4\omega'(0) \cos \gamma - \omega''(0)] \quad (21)$$

and

$$C_D = \frac{\pi}{2} \frac{b^2}{Uc} [\omega'(0)]^2 , \quad (22)$$

where the quantity  $c$  is the profile chord which is taken as unity in this work. The moment can be calculated after the complete solution has been found.

#### The Form of $\omega(\zeta)$ Near the Stagnation Point

This is also a well known result which we shall review briefly. The form of  $\omega$  near 0 is dominated by the fact that on a smooth contour  $\theta$  jumps by the amount  $\pi$ . In particular, as one traces the profile surface, starting at  $A_1$  in Fig. 1 and then passes through 0 while proceeding to  $A_2$ , the jump is a decrease in  $\theta$ . This is precisely the behavior exhibited by

where we have also made use of Eq. (18) because it applies to the wetted surface. But from Eq. (15) we have

$$\tau = \ln \frac{q}{U} = \ln \sqrt{1 - C_p} \quad ,$$

so that

$$ds = 2 \frac{b^2}{U} [(\cos \gamma - \cos \beta) \sin \beta \sqrt{1 - C_p(\beta)}] d\beta \quad (20)$$

on the wetted surface of the profile. As we have noted previously, the flow directions differ by  $\pi$  on either side of 0. Therefore, if the sign of  $dz$  is positive on the arc  $OA_2$ , it will be negative along arc  $OA_1$ . As a result of this difference  $ds$  might have a like sign change in these two regions. Just how this might occur depends on the form of  $\sqrt{1 - C_p(\beta)}$  in any particular case. Therefore, we will defer consideration of this question to a later place in the development.

#### Hydrodynamic Forces

The development of general formulae for the hydrodynamic forces on the profile depend upon certain properties of the function  $\omega(\zeta)$  which result from the previously noted fact that  $\omega(\zeta)$  is real when  $\zeta$  is real. For then one can apply Schwartz's principle of symmetry in order to write  $\omega(\bar{\zeta}) = \overline{\omega(\zeta)}$  and thereby obtain the analytic continuation of  $\omega(\zeta)$  into the lower half of the unit circle [6]. Thus we can write for a prescribed modulus,  $r_0 = |\zeta| < 1$ ,

$$\theta(\beta) - i\tau(\beta) = \theta(-\beta) + i\tau(-\beta) \quad ,$$

or

We can now use Eqs. (13), (14) and (15) in order to write

$$dz = dx + idy = \frac{b^2 e^{-\tau+i\theta}}{U} \left[ \frac{1}{2} \left( \zeta + \frac{1}{\zeta} \right) - \cos \gamma \right] \left( \zeta - \frac{1}{\zeta} \right) \frac{d\zeta}{\zeta} . \quad (17)$$

On the wetted surface  $\zeta = e^{i\beta}$  and Eq. (17) leads to

$$\left. \begin{aligned} d\bar{x} &= \frac{2b^2}{U} e^{-\tau} [\cos \gamma - \cos \beta] \sin \beta \cos \theta d\beta \\ \text{and} \\ d\bar{y} &= \frac{2b^2}{U} e^{-\tau} [\cos \gamma - \cos \beta] \sin \beta \sin \theta d\beta \end{aligned} \right\} . \quad (18)$$

Note that  $d\bar{y}/d\bar{x} = \tan \theta$  as it should if the wetted surface is to be a streamline. On the upper surface of the cavity  $\tau = 0$  and  $\arg \zeta = \pi$  so that Eq. (17) leads to

$$\left. \begin{aligned} dx_c &= \frac{b^2}{U} \cos \theta \left[ \frac{1}{2} \left( \zeta + \frac{1}{\zeta} \right) - \cos \gamma \right] \left( \zeta - \frac{1}{\zeta} \right) \frac{d\zeta}{\zeta} \\ dy_c &= \frac{b^2}{U} \sin \theta \left[ \frac{1}{2} \left( \zeta + \frac{1}{\zeta} \right) - \cos \gamma \right] \left( \zeta - \frac{1}{\zeta} \right) \frac{d\zeta}{\zeta} \end{aligned} \right\} \quad (19)$$

provided that  $-1 < \xi < 0$ .

Returning to Eq. (17), we can write the square of the arc length along the wetted surface as

$$(ds)^2 = dz d\bar{z} = \left\{ 2 \frac{b^2}{U} e^{-\tau} [\cos \gamma - \cos \beta] \sin \beta d\beta \right\}^2 ,$$

$$F = b^2 \left[ \cos \gamma - \frac{1}{2} \left( \zeta + \frac{1}{\zeta} \right) \right]^2 . \quad (10)$$

Then we introduce the complex velocity,

$$w = u - iv = \frac{dF}{dz} , \quad (11)$$

in order to write

$$w = qe^{-i\theta} = b^2 \left[ \cos \gamma - \frac{1}{2} \left( \zeta + \frac{1}{\zeta} \right) \right] \left( -\zeta + \frac{1}{\zeta} \right) \frac{1}{\zeta} \frac{d\zeta}{dz} , \quad (12)$$

or

$$wdz = dF = b^2 \left[ \frac{1}{2} \left( \zeta + \frac{1}{\zeta} \right) - \cos \gamma \right] \left( \zeta - \frac{1}{\zeta} \right) \frac{d\zeta}{\zeta} . \quad (13)$$

These quantities are now used to define the logarithmic hodograph or  $\omega$ -plane:

$$e^{-i\omega(\zeta)} = \frac{1}{U} \frac{dF}{dz} = \frac{w}{U} = \frac{q}{U} e^{-i\theta} = \exp \left[ \ln \frac{q}{U} - i\theta \right] . \quad (14)$$

Therefore we have

$$\omega(\zeta) = \theta + i \ln \frac{q}{U} = \theta + i\tau , \quad (15)$$

where  $\tau = \ln \frac{q}{U}$ . On the free streamlines  $q = U$  so that  $\tau = 0$  there. In the  $\zeta$ -plane, these free streamlines are on the real axis and at  $0'$  we know that  $\theta = 0$  also. Therefore,

$$\omega(0) = 0 \quad (16)$$

and  $\omega(\zeta)$  is real when  $\zeta$  is real. At the stagnation point  $q \rightarrow 0$  so that  $\tau \rightarrow -\infty$  there. The flow directions differ by  $\pi$  on either side of  $0$  and so the  $\omega$ -plane with the various corresponding boundaries can be represented as illustrated in Fig. 6.

One can now use the mapping

$$W = \frac{\sqrt{\phi_2} - \sqrt{\phi_1}}{2} (Z + \cos \gamma) , \tag{6}$$

where

$$\cos \gamma = \frac{a}{b} = \frac{\sqrt{\phi_1} - \sqrt{\phi_2}}{\sqrt{\phi_2} + \sqrt{\phi_1}} , \tag{7}$$

in order to map  $A_1$  into  $Z = +1$  and  $A_2$  into  $Z = -1$ . The point  $O$  maps into  $Z = \cos \gamma$  as shown in Fig. 4. The significance of the point  $C$ , also shown in this figure, is discussed later. Then the Joukowski transformation,

$$Z = -\frac{1}{2} \left( \zeta + \frac{1}{\zeta} \right) , \tag{8}$$

maps the upper half of the  $Z$ -plane onto the interior of the unit circle in the  $\zeta$ -plane. The inverse of this mapping must be

$$\zeta = -Z + \sqrt{Z^2 - 1} \tag{9}$$

in order to make the point  $O'$  map into the origin of the  $\zeta$ -plane. Various corresponding points are denoted by  $A_1$ ,  $A_2$  and  $O$  in Fig. 5. The arc of the unit semi-circle corresponds to the wetted surface. Coordinates on the wetted surface are given by  $\zeta = e^{i\beta}$  as shown. The stagnation point is at  $\beta = \gamma$ . The upper surface of the cavity is on the real axis between  $A_1$  and  $O'$  and the lower surface of the cavity is on the real axis between  $A_2$  and  $O'$  as marked in Fig. 5.

One can now use Eqs. (3) through (8) in order to write the composite of the preceding mappings as

$$\left. \begin{aligned}
 x_1 &= \frac{E^2}{U} \left[ \frac{\cos t_1}{t_1^2} - \frac{\sin t_1}{t_1} + \text{Ci}(t_1) \right] \\
 \text{and} \\
 y_1 &= \frac{E^2}{U} \left[ \frac{\sin t_1}{t_1^2} + \frac{\cos t_1}{t_1} + \text{Si}(t_1) - \frac{\pi}{2} \right]
 \end{aligned} \right\} \cdot \quad (37)$$

On the rest of the wetted surface, that is, on arc  $OA_2$  between the stagnation point and the tail, we know that  $\beta < \gamma$  and we put  $t = -t_2$ ,  $\gamma = \pi - \delta$  and  $\beta_2 = \pi - \xi_2$ . Then

$$t_2 = \frac{E}{b[\cos \delta - \cos \xi_2]} \cdot$$

In this case,  $\delta < \xi_2 < \pi$  and it follows that

$$\infty < t_2 < \frac{E}{b(1 + \cos \delta)} \cdot$$

Then we have

$$\left. \begin{aligned}
 x_2 &= \frac{E^2}{U} \left[ \frac{\cos t_2}{t_2^2} - \frac{\sin t_2}{t_2} + \text{Ci}(t_2) \right] \\
 \text{and} \\
 y_2 &= -\frac{E^2}{U} \left[ \frac{\sin t_2}{t_2^2} + \frac{\cos t_2}{t_2} + \text{Si}(t_2) - \frac{\pi}{2} \right]
 \end{aligned} \right\} \cdot \quad (38)$$

On the cavity surface  $A_1O'$  the integration starts at  $\zeta = -1$  and ends somewhere between  $\zeta = -1$  and  $\zeta = 0$ . Note that the value of  $t$  at  $\zeta = -1$  equals that of  $t_1$  when  $\beta = 0$ . So that if we put  $t = t_3$ ,  $\gamma = \pi - \delta$  and  $\zeta = -\zeta_3$ , we have

$$t_3 = \frac{E}{b \left[ \frac{1}{2} \left( \zeta_3 + \frac{1}{\zeta_3} \right) - \cos \gamma \right]}$$

then the upper cavity joins the nose arc of the wetted surface and its coordinates are

$$\left. \begin{aligned} x_3 &= \frac{E^2}{U} \left[ \frac{\cos t_3}{t_3} - \frac{\sin t_3}{t_3} + \text{Ci}(t_3) \right] \\ \text{and} \\ y_3 &= \frac{E^2}{U} \left[ \frac{\sin t_3}{t_3} + \frac{\cos t_3}{t_3} + \text{Si}(t_3) - \frac{\pi}{2} \right] \end{aligned} \right\} \quad (39)$$

In this case

$$0 < t_c < \frac{E}{b(1 - \cos \delta)}$$

Finally, the cavity surface from the trailing edge is obtained by putting  $t = -t_4$ ,  $\gamma = \pi - \delta$  and  $\zeta = \zeta_4$ , where  $0 < \zeta_4 < 1$ . Therefore

$$t_4 = \frac{E}{b \left[ \cos \delta - \frac{1}{2} \left( \zeta_4 + \frac{1}{\zeta_4} \right) \right]}$$

and

$$0 < t_4 < \frac{E}{b(1 + \cos \delta)} .$$

Then we have

$$x_4 = \frac{E^2}{U} \left[ \frac{\cos t_4}{t_4^2} - \frac{\sin t_4}{t_4} + \text{Ci}(t_4) \right]$$

and

$$y_4 = -\frac{E^2}{U} \left[ \frac{\sin t_4}{t_4^2} + \frac{\cos t_4}{t_4} + \text{Si}(t_4) - \frac{\pi}{2} \right]$$

(40)

As we found for the upper cavity, the lower cavity surface starts smoothly from the wetted surface.

Equations (37), (38), (39) and (40) will provide the shape of the wetted surface and the cavity surfaces for the simple complementary function of Eq. (33). However, these equations contain the undetermined ratio  $E^2/U$ . We shall consider the ratio  $E/b$ , which determines the strength of the complementary solution, as a parameter which we can prescribe -- at least for the time being. We also consider the value of  $\gamma$  (or  $\delta$ ) to be known. Therefore, we need to "scale" our results in order to obtain a profile of unit chord. Since we anticipate that the complementary function can produce a rounding of the wetted surface nose, the scaling procedure must account for this possibility. Accordingly, we shall need to determine explicitly the location of the apex of the wetted surface nose with respect to the profile chordline.

Figure 1 shows the chordline for the sharp-nose or for the round-nose case when the upper cavity separates at the leading edge with respect to the hydrofoil chord. The geometry for the rounded nose with the separation point on the upper wetted surface behind the apex of the wetted surface contour is illustrated in Fig. 7. The apex is located at the origin of  $\sigma, \eta$  coordinates in this illustration with the  $\eta$  axis being tangent to the contour at this point. Denote the  $x, y$  coordinates of this point by  $x_a, y_a$ . Then since the  $\sigma$ -axis is normal to the  $\eta$  axis, we see that at the apex the slope of the contour is

$$\frac{dy_a}{dx_a} = \tan \left( \frac{\pi}{2} - \alpha \right) = \cot \alpha \quad . \quad (41)$$

We will restrict our attention to those cases in which the apex is on the arc  $OA_1$ . Let  $t = t_1 = t_a$  at the apex. Then from the equations preceding Eq. (37), which define  $t_1$ , we have

$$t_a = \frac{E}{b(\cos \xi_a - \cos \delta)} \quad , \quad 0 < \xi_a < \delta \quad , \quad (42)$$

and Eq. (42) can then be used in Eqs. (37) to define  $x_a$  and  $y_a$  once the value of  $\xi_a$  (or  $\beta_a$ ) has been found. Thus, we must determine the unknowns  $E^2/U$  and  $\xi_a$  in terms of the prescribed quantities  $E/b$  and  $\delta$ (or  $\gamma$ ). Two conditions are available for this purpose. The first is given by Eq. (41). The second will be that the profile has a unit chord.

An alternate form of Eq. (41) is

and

$$\left. \begin{aligned} \cos \alpha &= \sin t_a \\ \sin \alpha &= \cos t_a \end{aligned} \right\} \quad , \quad (43)$$

which follows from the complex equation just above Eq. (36) when we put  $t = t_a$ . We will use Eq. (43) as the appropriate expression for the slope of the foil contour at the apex. Now let us differentiate Eq. (1) so that

$$d(\sigma + in) = e^{i\alpha} dz .$$

Then from the complex equation just preceding Eq. (36) we have

$$e^{-i\alpha} d(\sigma + in) = -\frac{2E^2}{U} \frac{1}{t^3} e^{it} dt . \quad (44)$$

Starting from 0 where  $(\sigma, n) = (\sigma_0, n_0)$ , we integrate Eq. (44) to  $A_2$ , where  $(\sigma, n) = (1, 0)$ . This step gives

$$e^{-i\alpha}(1 - \sigma_0 - in_0) = \frac{E^2}{U} \left\{ \left[ \frac{\cos t_t}{t_t^2} - \frac{\sin t_t}{t_t} + Ci(t_t) \right] - i \left[ \frac{\sin t_t}{t_t^2} + \frac{\cos t_t}{t_t} + Si(t_t) - \frac{\pi}{2} \right] \right\} ,$$

where

$$t_t = \frac{E}{b(1 + \cos \delta)} ,$$

corresponding to  $t_2$  with  $\xi_2 = \pi$  in Eqs. (38). Next we can use Eqs. (37) with  $\xi_1 = \xi_a$  and  $t_1 = t_a$  or

$$t_a = \frac{E}{b(\cos \xi_a - \cos \delta)}$$

at the apex in order to integrate Eq. (44) from 0 to the apex along the arc  $OA_1$ . This step results in

$$- e^{-i\alpha}(\sigma_0 + i\eta_0) = \frac{E^2}{U} \left\{ \left[ \frac{\cos t_a}{t_a^2} - \frac{\sin t_a}{t_a} + \text{Ci}(t_a) \right] + i \left[ \frac{\sin t_a}{t_a^2} + \frac{\cos t_a}{t_a} + \text{Si}(t_a) - \frac{\pi}{2} \right] \right\} .$$

Eliminating the sum  $\sigma_0 + i\eta_0$  from these two equations, we get

$$\text{and } \left. \begin{aligned} \frac{U}{E^2} \cos \alpha &= F - f(t_a) \\ \frac{U}{E^2} \sin \alpha &= G - g(t_a) \end{aligned} \right\} . \quad (45)^*$$

In Eqs. (45) we have

---

\*The F introduced here is not to be confused with  $F = \phi + i\psi$  from Eq. (2).

$$\left. \begin{aligned}
 F &= \frac{x_t U}{E^2} = \frac{\cos t_t}{t_t^2} - \frac{\sin t_t}{t_t} + \text{Ci}(t_t) \\
 G &= \frac{y_t U}{E^2} = \frac{\sin t_t}{t_t^2} + \frac{\cos t_t}{t_t} + \text{Si}(t_t) - \frac{\pi}{2}
 \end{aligned} \right\} \quad (46)$$

and

which contain known quantities because  $t_t$  is known. The remaining pair of functions,

$$\left. \begin{aligned}
 f(t_a) &= \frac{\cos t_a}{t_a^2} - \frac{\sin t_a}{t_a} + \text{Ci}(t_a) \\
 g(t_a) &= \frac{\sin t_a}{t_a^2} + \frac{\cos t_a}{t_a} + \text{Si}(t_a) - \frac{\pi}{2}
 \end{aligned} \right\} , \quad (47)$$

and

contains  $t_a$  which depends upon the unknown,  $\beta_a = \pi - \xi_a$ . Thus, Eqs. (45) are two simultaneous equations containing the quantities  $U/E^2$ ,  $\alpha$  and  $\beta_a$  which must be determined. Therefore, Eqs. (43) and (45) form a determinate system which can be solved by iteration. In order to do this, we can write the complete system as

$$\tan \alpha = \frac{G - g(t_a)}{F - f(t_a)} , \quad (48)$$

$$\cot t_a = \tan \alpha \tag{49}$$

and

$$\frac{U}{E^2} = \frac{F - f(t_a)}{\cos \alpha} = \frac{G - g(t_a)}{\sin \alpha} \tag{50}$$

In the derivation of this system we have assumed that the apex,  $z_a$ , is on the arc  $OA_1$ . On the other hand, we specify the quantities  $E/b$  and  $\gamma = \pi - \delta$ . We must now determine whether or not our assumption regarding the location of  $z_a$  can restrict possible choices for the parameters  $E/b$  and  $\delta$ . In particular, we recall that, as is true for the quantity  $\xi_1$ , we must also require that  $0 < \xi_a < \delta$ , as noted in Eq. (44). The limiting condition, corresponding to the coincidence of the apex and cavity separation point at the nose of the profile corresponds to  $\xi_a = 0$ . In this case, the smallest value of  $t_1$  for any choice of  $E/b$  will be found when

$$t_a \Big|_{\min} = \frac{E}{b(1 - \cos \delta)} \tag{51}$$

On the other hand, by inspection Eqs. (46) and (47), we see that the largest values of  $f$  and  $g$  are found for  $t_a = t_{\min}$ . The values of  $F$  and  $G$  are also obtained from the smallest value of  $t_2$  because  $t_t$  is calculated from  $t_2$  with  $\xi_2 = \pi$ , namely:

$$t_t = \frac{E}{b(1 + \cos \delta)} \tag{52}$$

Let us compare the values of  $F$  with  $f$  and  $G$  with  $g$ . Suppose that  $E/b$  is selected so that  $\cos t_a \approx \cos t_t \approx 1$ ,  $\sin t_a \approx t_a$  and  $\sin t_t \approx t_t$ . Let  $\delta \ll 1$ . In this case we can see that

$$\frac{F}{f} = \left( \frac{t_a|_{\min}}{t_t} \right)^2 = \left( \frac{2}{\delta} \right)^4 \left( 1 - \frac{2\delta^2}{3} \right) \quad \text{and} \quad \frac{G}{g} = \left( \frac{t_a|_{\min}}{t_t} \right) = \left( \frac{2}{\delta} \right)^2 \left( 1 - \frac{\delta^2}{6} \right) .$$

For example, if  $\delta = .1$ , we would estimate  $F/f \sim (20)^4$  and  $G/g \sim (20)^2$ . These estimates imply that both  $E/b$  and  $\delta$  are significantly smaller than unity.

In the applications contemplated,  $E/b$  will probably be less than unity although  $\delta$  might conceivably approach or exceed unity. Therefore, we shall consider the ratio,

$$\frac{t_a|_{\min}}{t_t} = n = \frac{1 + \cos \delta}{1 - \cos \delta} , \quad n > 1 ,$$

which permits us to consider roughly the ratios of  $F$  to  $f$  and of  $G$  to  $g$  for various values of  $\delta$ . In particular, we can solve for  $\cos \delta$  and obtain

$$\cos \delta = \frac{n - 1}{n + 1} ,$$

which permits us to plot a curve of  $n = (t_a|_{\min}/t_t)$  versus  $\delta$  as shown in Fig. 8. This curve illustrates the effect that the choice of stagnation point location has on the ratio,  $n$ . The value of  $n$  in turn gives a rough indication of how large the ratios  $F/f$  and  $G/g$  will be.

It appears for most cases that these ratios will be very large and one need not solve Eqs. (48) and (49) by iteration. Instead one can obtain an accurate value of  $\alpha$  from

$$\tan \alpha \approx \frac{G}{F} \quad (48a)$$

and he can then determine  $U/E^2$  from

$$\frac{U}{E^2} = \frac{F}{\cos \alpha} \quad (50a)$$

Should cases arise in which Eqs. (48a) and (50a) are not accurate, they can be used advantageously to start the iteration. In order to illustrate these points and in order to show a profile shape derived from the complementary solution, we have prepared the following numerical example.

We started the calculation by selecting  $\delta = 70^\circ$  and  $E/b = .01$ . Figure 8 shows that  $n \approx 2$ . The values  $t_a \Big|_{\min} = .01520$  and  $t_t = .00745$  follow from the formulae for these quantities. From Eqs. (46) we find that  $F = 18,004$  and  $G = 266.83$ . Equations (48a) and (50a) lead to  $\tan \alpha = .01482$  and  $U/E^2 = 18,006$ . From the formulae just after Eq. (35) we have for the cavity drag due to a profile of unit chord

$$C_{D_c} = 2\pi \frac{E^2}{U} = .00035$$

as the contribution for this point-drag profile. The value of  $t_a$  can now be found from Eq. (49). It is  $t_a = 1.556$ . Equation (42) can now be used to find that  $\xi_a = 69.61^\circ$ . Note that for this case the apex is almost coincident with the stagnation point. Because Eq. (34a) shows the complementary function to be at the stagnation point this result is expected. The fact that the apex is not exactly at  $\delta = 70^\circ$  is due only to the inclination,  $\alpha = .85^\circ$ , between the chord line and the x axis. Once  $U/E^2$  has been found, the values of  $x_t$  and  $y_t$  can be found from Eqs. (46). The values are  $x_t = .99989$  and  $y_t = -.01482$ . Now one can

use the conditions that in Eqs. (1),  $(x_t, y_t) \leftrightarrow (\sigma=1, \eta=0)$  and  $(x_a, y_a) \leftrightarrow (\sigma=0, \eta=0)$ . These lead to a system of equations from which  $\sigma_0$  and  $\eta_0$  can be eliminated and one finds that

$$x_a = x_t - \cos \alpha = x_t - \sin t_a ,$$

$$y_a = y_t + \sin \alpha = y_t + \cos t_a .$$

When the above values of  $x_t$  and  $\alpha$  were used in these equations, the values of  $x_a$  and  $y_a$  were found to be zero to within five decimal places. This result is consistent with the location of  $\xi_a$  noted previously. Continuing with Eqs. (1), we can use the fact that  $x_a = y_a = 0$  to see that it must also follow that  $\sigma_0 = \eta_0 = 0$ . Accordingly, the form of Eqs. (1) for the present calculations is

$$\sigma = .99989x - .014796y ,$$

$$\eta = .014796x + .999989y .$$

The next phase of the calculations is the evaluation of the equations for the wetted surface and cavity contours in accordance with Eqs. (37), (38) and (39). The result of these calculations is shown in Fig. 9. In this figure, the chordline distance,  $\sigma$ , has been labeled as X and the ordinate,  $\eta$ , has been labeled as Y. Note that the Y-scale is magnified five times compared to that of the X-scale. The trailing edge of the wetted surface is at  $X = 1$ . The upper surface separation point is at  $\sigma = X = .240$ . The cavity thickness at  $X = 1$  is  $Y = T = .02980$ . This point is marked to the same scale as the X-scale by the dot and the line at  $X = 1$  in order to give an idea of the actual thickness of this example of a point-drag profile. Finally we can calculate the value of  $\zeta_c(1)$

in this example in order to compare it with the values found previously for the flat-plate. It is found from the value of  $\tau_c = (E/b)/[(\zeta_c + 1/\zeta_c)/2 \cos \gamma]$  at  $\sigma = 1$ . The calculations indicated give  $\zeta_c(1) = .3290$  which is roughly two times the values of Table 1.

Our desire to retain as much simplicity as possible in the preceding analysis of the complementary function has caused us to place the point-drag singularity at the stagnation point. This restriction on the location of the point of application has allowed us to show that such a solution exists, that it definitely leads to a smoothly rounded profile nose and that it will cause an incremental thickening of the cavity depending on its strength, E. Of course, we need not restrict ourselves to the stagnation point as being the location of the point-drag singularity.

For example, suppose we choose some other point C on the wetted surface. Such a point is illustrated in Fig. 5 and it happens to be located between the upper cavity separation point and the stagnation point, although C could just as well be at some other wetted-surface location. The main idea is that now  $\beta = \gamma_c$  at the location of the point-drag singularity and if we simply replace Eq. (34a) by the modified expression,

$$\omega_c(\zeta) = \frac{E}{b[\cos \gamma_c - \frac{1}{2}(\zeta + \frac{1}{\zeta})]} = \frac{-2E\zeta}{b(\zeta - e^{i\gamma_c})(\zeta - e^{-i\gamma_c})}, \quad (34b)$$

we still have a function which satisfies those conditions needed for a complementary solution. It is clear that in the  $\zeta$ -plane,  $\omega_c(1) = 0$ . Moreover, when  $\zeta$  is real  $\omega_c$  is real and on the unit circle  $\tau_c = 0$  everywhere except possibly at the simple poles,  $\zeta = e^{\pm i\gamma_c}$ . From Eqs. (21) and (22) it follows that

$$C_{D_c} = 2\pi \frac{E^2}{Uc} \quad (51)$$

as before. On the other hand, because of the displacement of the point C away from 0, a lift force is produced and we find that now

$$C_{L_c} = \frac{8\pi bE}{Uc} \sin \frac{\gamma + \gamma_c}{2} \sin \frac{\gamma - \gamma_c}{2} = \frac{8\pi bE}{Uc} \sin \frac{\delta_c + \delta}{2} \sin \frac{\delta_c - \delta}{2}, \quad (52)$$

where  $\gamma = \pi - \delta$  and  $\gamma_c = \pi - \delta_c$  in accordance with previous convention. The profile chord,  $c$ , should be set at unity in Eqs. (51) and (52). Equation (52) shows that  $C_{L_c} = 0$  when  $\delta_c = \delta$ . However,  $\delta_c < \delta$  when the point C moves toward the point  $A_1$  and a negative lift results. In the limit as  $\delta_c \rightarrow 0$ , we have

$$C_{L_c} = -\frac{8\pi bE}{Uc} \sin^2 \frac{\delta}{2}.$$

If C is between 0 and  $A_2$  a positive lift is produced and in the limit when C is coincident with  $A_2$  we have

$$C_{L_c} = \frac{8\pi bE}{Uc} \cos^2 \frac{\delta}{2}.$$

If one were to let  $E$  be negative the sign of the foregoing trends with respect to  $C_L$  would be reversed. However, we must insist that  $E > 0$  because this function produces a thickening of the cavity and because then  $\omega'_c(0) = -2E/b$ . Similarly, we have also found that  $\omega'_0(0) = 0.2 \sin \gamma$ . Thus, the effect of adding  $\omega_0$  and  $\omega_c$  increases the net drag. Neither of these functions can act to reduce it. Accordingly, we shall take Eq. (34b) as the appropriate form of the eigensolution which has been sought.

Conclusions

The chief finding of this paper is that one can construct many eigensolutions for the exact inverse problem of two-dimensional cavity flow at zero cavitation number. From among these, we have chosen that eigensolution which appears to offer the least disturbance to the upstream flow field inclination of any cavity flow which does not already include a point-drag solution as one of its elements. This particular choice also seems to offer the greatest analytical convenience. The physical conditions satisfied by this eigensolution are:

- (1) At points on the cavity and on the wetted surface of the profile, the flow velocity is equal in magnitude to the free-stream velocity.
- (2) The point-drag solution vanishes at infinity, but it does have an integrable singularity on the profile surface.
- (3) This function produces no additional flow inclination on the entire upstream stagnation streamline.

A specific example of the flow geometry represented by an isolated eigensolution has been given above to show how this function can produce round-nosed profiles. In general, it is found that the point-drag solution produces a widening of the cavity which is directly proportional to its strength. An incremental cavity drag accompanies this widening and this drag is proportional to the square of the eigensolution strength. No lift is produced by the point-drag function when its location coincides with that of the stagnation point on the profile surface. In contrast to the linearized theory, the complementary function singularity need not be at the stagnation point. In these cases, the incremental cavity drag is not changed from its value when the singularity is at the stagnation point.

But when the singularity is located between the stagnation point and the upper separation point a negative incremental lift is produced. If the singularity is on the lower surface, downstream of the stagnation point, a positive lift increment is found.

As a result of these findings, it appears that an eigensolution exists for the nonlinear theory of cavity flow at zero cavitation number and that it is now most likely that a similar eigensolution can be found for such fully cavitating flows at cavitation numbers which are greater than zero. The results found so far suggest that the nonlinearized theory and the linearized theories parallel one another very closely as far as the nature of the point drag solution are concerned. But the present results exhibit some features which are lost when the process of linearization is applied in the linearized formulation. Finally, the way is now clear to augment the method of Levi Civita by adding in the eigensolution,  $\omega_c$ , in order to formulate an exact inverse theory which permits one to control the cavity thickness and to prescribe the wetted-surface pressure distribution simultaneously.

References

1. Yim, B and L. Higgins, "A Nonlinear Design Theory of Supercavitating Cascades," Transactions of the ASME, Journal of Fluids Engineering, Vol. 97, Series I, No. 4, p. 430 (December 1975).
2. Khrabov, I. A., "Plane Problems of Cavitation Flow Around an Oblique Cascade of Profiles," Izvestiya Akademii Nauk SSSR, Mekhanika Zhidkosti i Gaza, No. 3, pp. 149-152 (May-June 1975). Translated: Plenum Publishing Corporation, 227 West 17<sup>th</sup> Street, New York (1977).
3. Furuya, O., "Exact Supercavitating Cascade Theory," Transactions of the ASME, Journal of Fluids Engineering, Vol. 97, Series I, No. 4, p. 430 (December 1975).
4. Durand, W. F. (Ed.), Aerodynamic Theory, Vol. II, by Th. Von Karman and J. M. Burgers, Dover Publications, Inc., New York, pp. 336-339 (1963).
5. Gurevich, M. I., Theory of Jets in Ideal Fluids, Academic Press, New York, pp. 131-143 (1965).
6. Woods, L. C., The Theory of Subsonic Plane Flow, Cambridge University Press, London, pp. 443-454 (1961).
7. Milne-Thomson, L. M., Theoretical Hydrodynamics, Fifth Edition, The MacMillan Press, Ltd., London, pp. 338-348 (1968).
8. Yoshihara, H., "Optimum Fully Cavitated Hydrofoils at Zero Cavitation Number," Journal of Aircraft, Vol. 3, No. 4, p. 372 (1966).
9. Parkin, B. R. and R. S. Grote, "Inverse Methods in the Linearized Theory of Fully Caviting Hydrofoils," Transactions of the ASME, Journal of Basic Engineering, Vol. 86, Series D, No. 4 (December 1964).

10. Parkin, B. R. and J. Fernandez, "A Third Procedure for Linearized Fully-Cavitating Hydrofoil Section Design," ARL Technical Memorandum, File No. TM 77-186, Applied Research Laboratory, The Pennsylvania State University (5 July 1977).
11. Parkin, B. R., "An Extended Linearized Inverse Theory for Fully Cavitating Hydrofoil Section Design," J. Ship Research, p. 260 (December 1979).  
  
\_\_\_\_\_, "Hydrodynamic Trends from a Generalized Design Procedure for Fully Cavitating Hydrofoil Sections," J. Ship Research, p. 272 (December 1979).
12. Lamb, Sir Horace, Hydrodynamics, Sixth Edition, Dover Publications, New York, pp. 102-103 (1945).
13. Parkin, B. R., "Munk Integrals for Fully Cavitating Hydrofoils," J. of the Aerospace Sciences, Vol. 29, No. 7, p. 775 (July 1962).

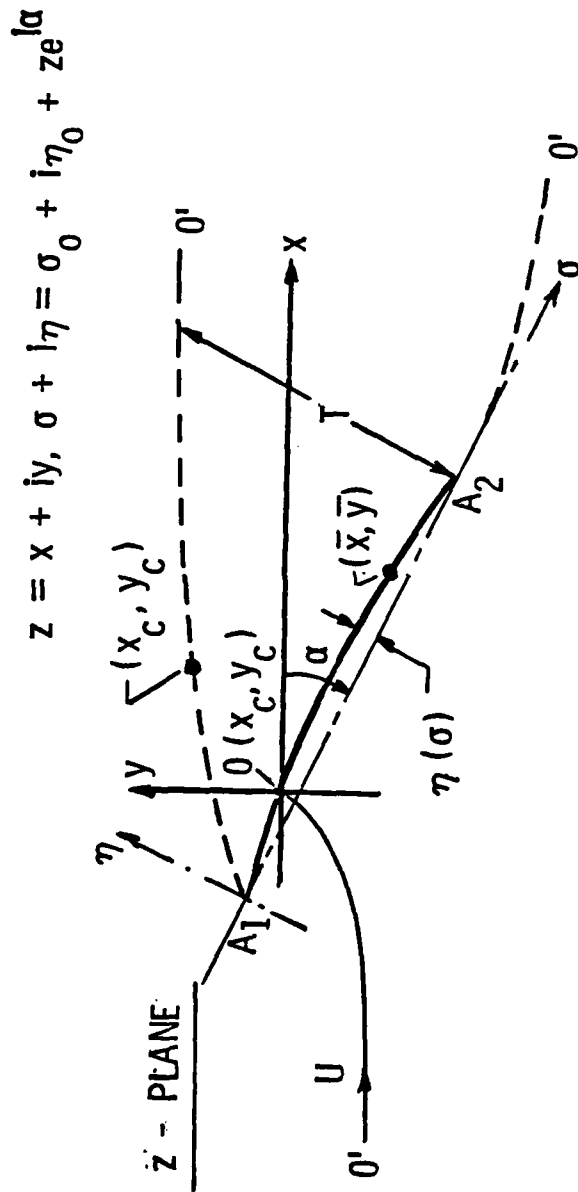


Figure 1. Profile and cavity geometry in the physical or z-plane at zero cavitation number.

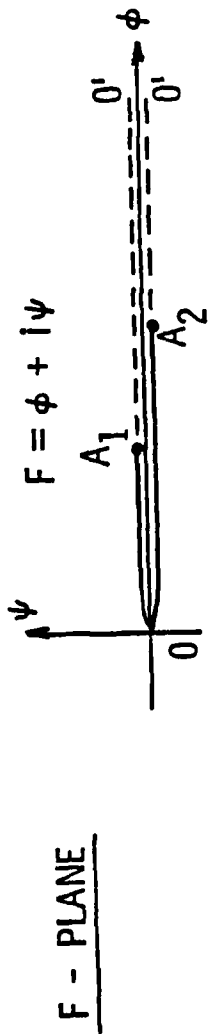


Figure 2. Profile and cavity surfaces at zero cavitation number in the plane of the complex potential,  $F = \phi + i\psi$ .

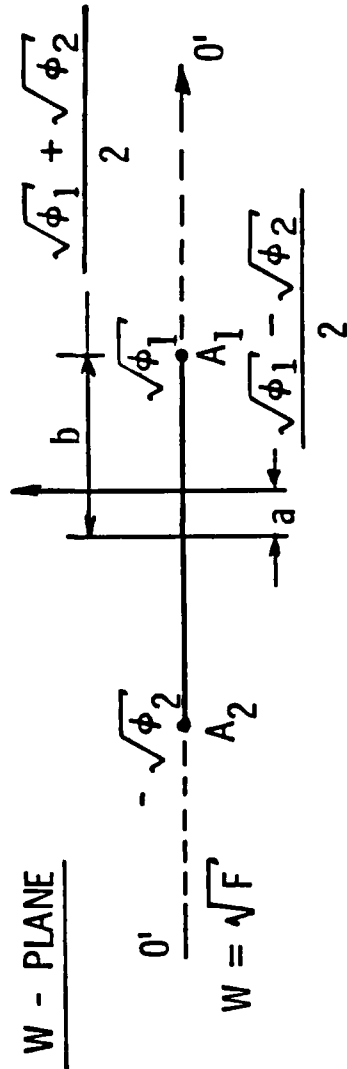


Figure 3. The mapping  $W = \sqrt{F}$  maps the flow outside the cut in the F plane into the upper half W plane.



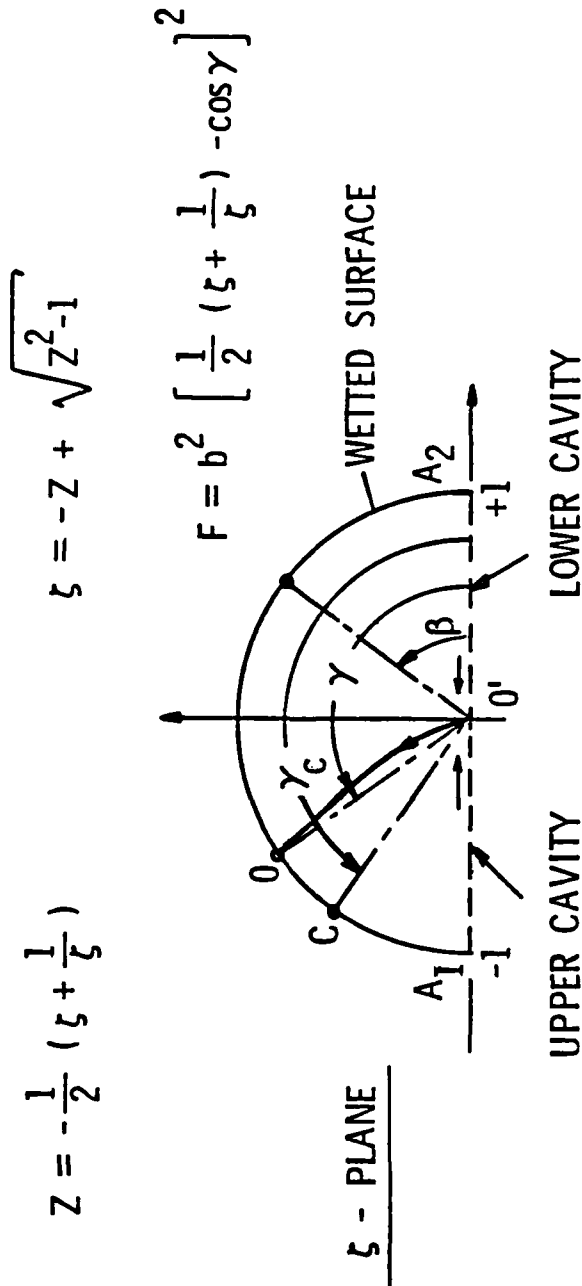


Figure 5. The Joukowski transformation maps the flow from the upper half of the Z-plane into the interior of the upper unit semi-circle with the point at infinity at the origin.

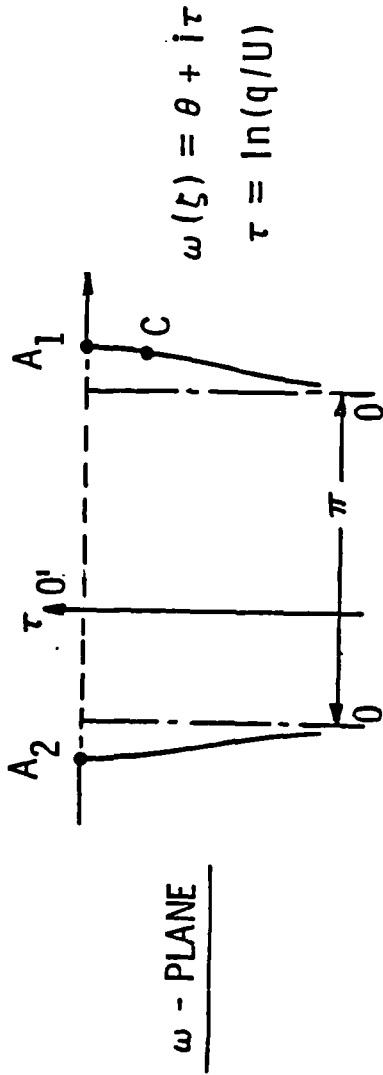


Figure 6. Schematic diagram of the complex logarithmic hodograph in the  $\omega$ -plane.

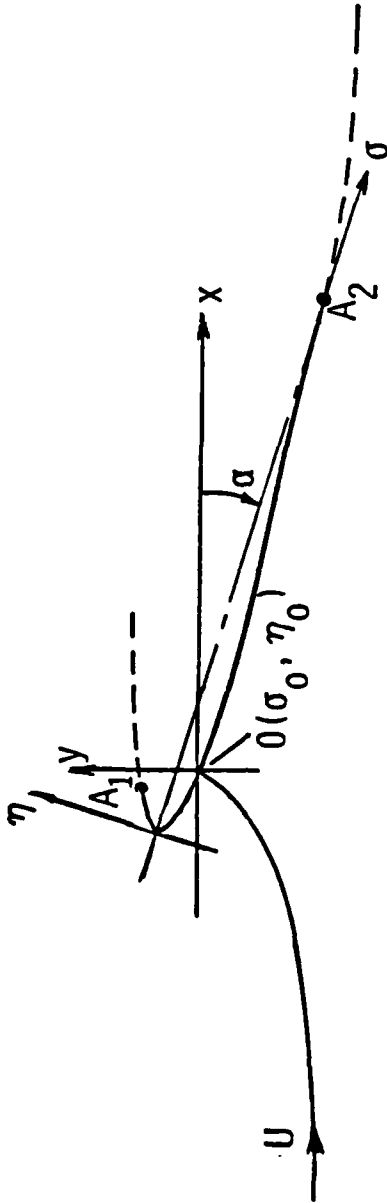


Figure 7. The geometry of a round-nosed profile of unit chord showing the origin of  $\sigma - \eta$  coordinates at the apex of the wetted surface corresponding to  $(x_a, y_a)$  in  $z$ -plane coordinates.

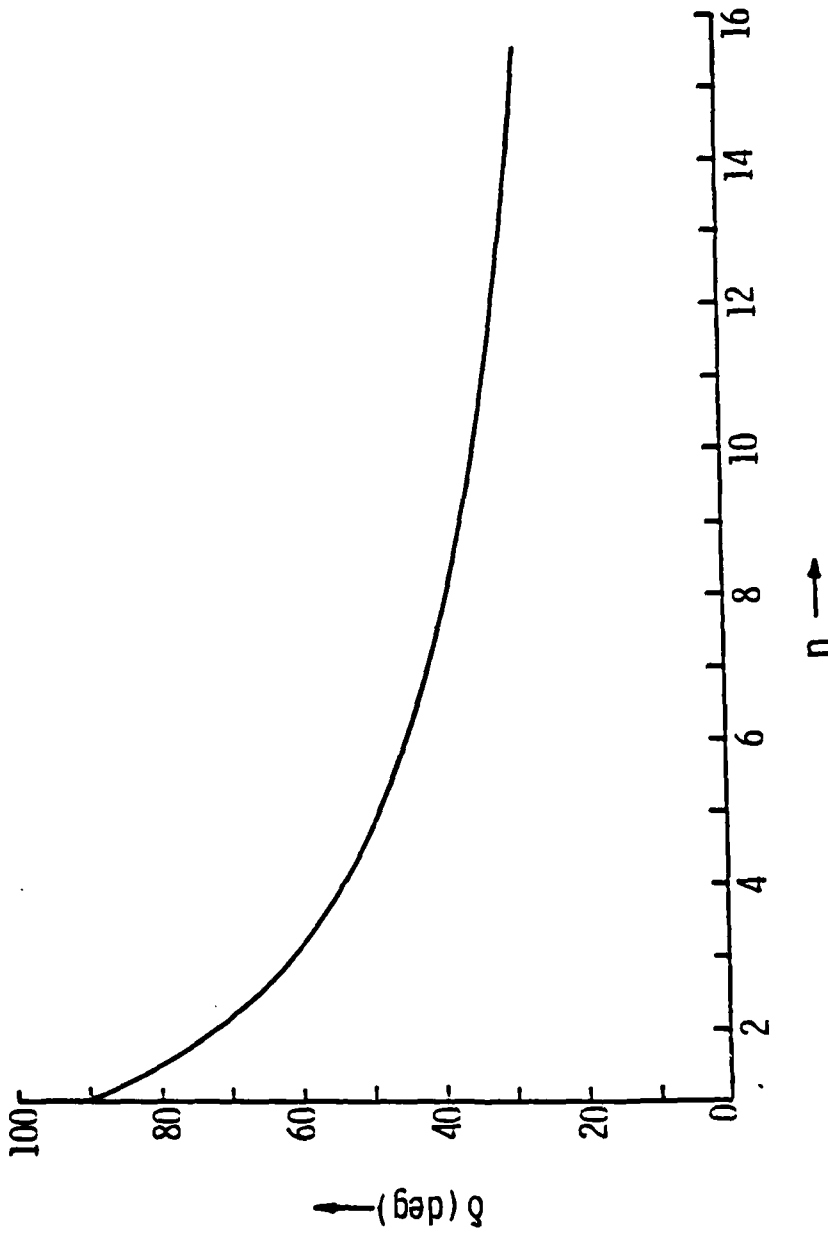


Figure 8. Angular location,  $\delta$ , of the stagnation point vs the parameter  $n$  for the isolated eigensolution.

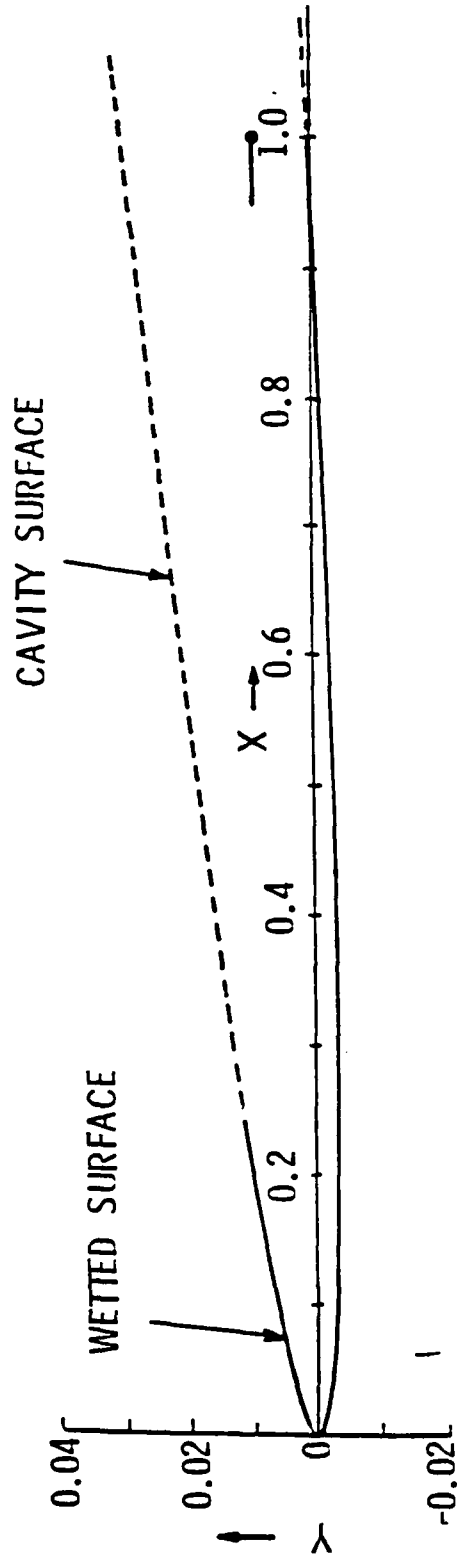


Figure 9. The profile and cavity contours produced by an isolated eigenfunction of strength  $\frac{E}{b} = .01$  at the stagnation point  $\delta = 70^\circ$  which produces a cavity drag  $C_{Dc} = .0035$  and cavity thickness  $T = .0298$ . Note the distortion of the vertical scale in the plot. The line and dot at  $X = 1$  show the true geometry when the vertical and horizontal axes have the same scale.

DISTRIBUTION LIST FOR UNCLASSIFIED TECHNICAL MEMORANDUM 85-16,  
by B. R. Parkin, dated 25 January 1985

Defense Technical Information  
Center  
5010 Duke Street  
Cameron Station  
Alexandria, VA 22314  
(Copies 1 through 6)

Commanding Officer  
David W. Taylor Naval Ship  
Research & Development Ctr.  
Department of the Navy  
Bethesda, MD 20084  
Attention: M. Tod Hinkel  
Code 1504  
(Copies 7 through 12)

Commander  
Naval Sea Systems Command  
Department of the Navy  
Washington, DC 20362  
Attention: T. E. Peirce  
Code NSEA-63R31  
(Copy No. 13)

Director  
Applied Research Laboratory  
The Pennsylvania State University  
Post Office Box 30  
State College, PA 16804  
Attention: M. L. Billet  
(Copy No. 14)

Director  
Applied Research Laboratory  
The Pennsylvania State University  
Post Office Box 30  
State College, PA 16804  
Attention: L. R. Hettche  
(Copy No. 15)

Director  
Applied Research Laboratory  
The Pennsylvania State University  
Post Office Box 30  
State College, PA 16804  
Attention: J. W. Holl  
(Copy No. 16)

Director  
Applied Research Laboratory  
The Pennsylvania State University  
Post Office Box 30  
State College, PA 16804  
Attention: B. R. Parkin  
(Copy No. 17)

Director  
Applied Research Laboratory  
The Pennsylvania State University  
Post Office Box 30  
State College, PA 16804  
Attention: GTWT Files  
(Copy No. 18)

Director  
Applied Research Laboratory  
The Pennsylvania State University  
Post Office Box 30  
State College, PA 16804  
Attention: ARL/PSU Library  
(Copy No. 19)

**END**

**FILMED**

4-85

**DTIC**